JOURNAL OF SYNCHROTRON RADIATION

ISSN 1600-5775

Ground electronic state description of thiourea coordination in homoleptic Zn^{2+}, Ni^{2+} and Co^{2+} complexes using sulfur *K*-edge X-ray absorption spectroscopy

Matt S. Queen,[a] Farideh Jalilehvand[b] and Robert K. Szilagyi[c]*‡

[a]Biological and Physical Sciences, Montana State University Billings, Billings, MT 59101, USA, [b]Department of Chemistry, University of Calgary, Calgary, AB T2N 1N4, Canada, and [c]Department of Chemistry and Biochemistry, Montana State University, 700 Cleveland Street, Bozeman, MT 59717, USA. *Correspondence e-mail: szilagyi@montana.edu

Received 26 May 2021
Accepted 12 August 2021

Edited by S. M. Heald, Argonne National Laboratory, USA

‡ Current address: Department of Chemistry, The University of British Columbia – Okanagan, 3187 University Way, Kelowna, BC V1V 1V7, Canada.

Keywords: sulfur *K*-edge XANES; S-donor ligand; transition dipole integral; metal–ligand bond covalency; ground electronic state; molecular orbital composition; versatile S-donor ligand.

Supporting information: this article has supporting information at journals.iucr.org/s

Sulfur *K*-edge X-ray absorption spectroscopy (XAS) was employed to experimentally characterize the coordinative bond between the thiourea (TU) or thiocarbamide ligand and transition metal (TM) ions Zn^{2+}, Co^{2+} and Ni^{2+} in distorted tetrahedral and octahedral homoleptic coordination environments. Comparisons of XAS spectra of the free TU ligand and $[Zn(TU)_4]^{2+}$, $[Co(TU)_4]^{2+}$ and $[Ni(TU)_6]^{2+}$ complexes clearly identify spectral features unique to TM^{2+}–S(TU) bonding. Quantitative analysis of pre-edge intensities describes the covalency of Ni^{2+}—S(TU) and Co^{2+}—S(TU) bonding to be at most 21% and 9% as expressed by the S 3*p* contributions per TM 3*d* electron hole. Using relevant Ni^{2+} complexes with dithiocarbamate and thioether ligands, we evaluated the empirical S $1s \rightarrow 3p$ transition dipole integrals developed for S-donor ligands and their dependence on heteroatom substitutions. With the aid of density functional theory-based ground electronic state calculations, we found evidence for the need of using a transition dipole that is dependent on the presence of conjugated heteroatom (N) substitution in these S-donor ligands.

1. Introduction

Thiourea $[(H_2N)_2CS$; TU] or thiocarbamide can be considered as a structurally versatile ligand in coordination complexes due to its simultaneous σ-donor and π-acid characters that are manifested in the ability of TU to form hydrogen tautomers and electron resonance structures (Scheme 1). A thione or thiocarbonyl (C═S) functional group is generally not considered to be a good donor to transition metal (TM) ions, yet TU forms well defined mononuclear complexes with zinc(II) (Vega *et al.*, 1978), cobalt(II) (Cotton *et al.*, 1964) and nickel(II) ions (Weininger *et al.*, 1969). Formally, in $[Ni(TU)_6]^{2+}$ TU ligands coordinate *via* sulfur lone pairs in σ interactions forming a close-to-octahedral ligand environment around the nickel(II) ion. In the $[Co(TU)_4]^{2+}$ and $[Zn(TU)_4]^{2+}$ complexes, the sulfur lone pairs are involved in pseudo-σ/π donor interactions with the TM which result in distorted tetrahedral coordination. The thiocarbonyl coordination and corresponding ground electronic state of the nickel(II)–TU complex have been studied indirectly by infrared spectroscopy (Yamaguchi *et al.*, 1958; Kumler & Fohlen, 1942; El-Bahy *et al.*, 2003). These studies showed that N—H symmetric and asymmetric stretching modes as well as the N—C—N bending modes were shifted to higher energy in coordinated TU relative to the free TU ligand. These blue shifts in the IR spectra were attributed to an increase in the double-bond

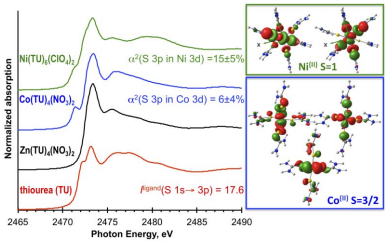

character between the nitrogen and carbon upon TU coordination. According to Lewis structure descriptions, the resonance structure with thiolate character (Scheme 1, left-hand side) becomes dominant when TU is coordinated to a TM ion compared with the free ligand (Scheme 1, middle) with thione character. When considering tautomerism and TU interaction with Lewis acids, resonance structures (Scheme 1, right-hand side) rationalize the stability of TM complexes with both the C–S$^-$ and the –NH$^-$ functional groups coordinated (*e.g.* Watson *et al.*, 1991; Fritz *et al.*, 1994; Seitz *et al.*, 1994).

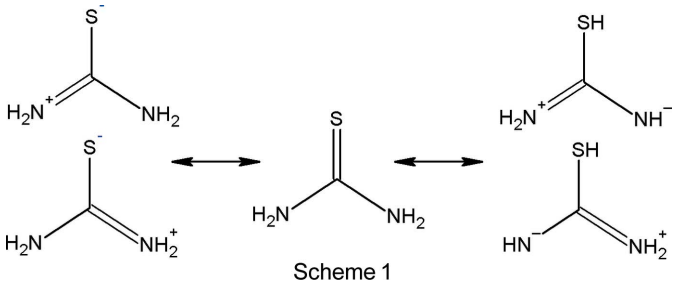

Scheme 1

In this study, we exemplify how sulfur *K*-edge X-ray absorption near-edge spectroscopic (S *K*-XANES) features can be directly correlated with the ground electronic state, despite the fact that X-ray absorption spectroscopy (XAS) is a core-level excited state technique. This study coincides with the 'pearl anniversary' of the seminal paper by Solomon, Hodgson and Hedman (Hedman *et al.*, 1990) that laid the foundation for the quantitative interpretation of XANES pre-edge feature intensities in terms of molecular orbital (MO) composition. We will demonstrate the MO-based approach by employing a spectrochemical series of the free TU ligand and its representative complexes with zinc(II), nickel(II) and cobalt(II) in two different coordination environments. Hybrid density functional theory-based (DFT) ground electronic state calculations were utilized to aid the spectral assignments and interpretation of data.

Specifically, S *K*-XANES is an experimental technique for quantitatively determining the covalency of metal–S(ligand) bonds (Solomon *et al.*, 2005). Tender X-ray radiation in the 2.4–2.9 keV energy range either excites S 1*s* core electrons into unoccupied S 3*p*/4*p*-based molecular orbitals or ionizes the electrons into the continuum. Ionization gives rise to an edge feature at *K*-shell excitations, which is superimposed with the highest energy and often ill-resolved bound-state excitations involving S 4*p* orbitals (Queen *et al.*, 2013). The X-ray photons with energy below the S 1*s* ionization threshold give rise to intense, dipole-allowed excitations into unoccupied *M*–S(ligand) antibonding (pre-edge) and C—S antibonding (rising-edge) orbitals of an S-donor ligand. The intensity of these transitions is proportional to the S 3*p* atomic orbital character of an experimentally probed molecular orbital, which can be expressed by an empirical transition dipole expression (Shadle *et al.*, 1995) in equation (1):

$$D_0 = \frac{1}{3}\frac{h}{N}\alpha^2 I(\mathrm{S}\ 1s \rightarrow 3p), \qquad (1)$$

where D_0 is the normalized, integrated pre-edge intensity (arbitrary unit), h is the number of electron holes probed, N is the number of sulfur absorbers per molecule and the 1/3 factor is due to the angular part of the transition dipole integral for $1s \rightarrow 3p$ excitations. The term $I(\mathrm{S}\ 1s \rightarrow 3p)$ is commonly referred to as the transition dipole integral (Shadle *et al.*, 1993), with considerable dependence on sample preparation protocol, beamline X-ray optics and detection method,[1] hence it has an empirical nature. The term α^2 represents the S 3*p* atomic orbital character in the absorber molecular orbital per electron hole, giving rise to spectral intensity D_0. In practice, $I(\mathrm{S}\ 1s \rightarrow 3p)$ corresponds to an empirical proportionality constant that connects the experimental peak intensities with adsorber atom-based orbital compositions. A loose analogy for the physical meaning of α^2 and $I(\mathrm{S}\ 1s \rightarrow 3p)$ is the consideration of a fraction of electron density that is localized on the S adsorber associated with a frontier unoccupied molecular orbital that gives rise to the experimentally probed excited state. In our earlier work (Queen *et al.*, 2013), a general method was proposed for deriving experimental transition dipole integrals using free ligands as reference points. The dipole integral was expressed as a function of the S effective nuclear charge [Z_{eff}(S)] experienced by the 1*s* core orbital in a given compound (Neese *et al.*, 1999). A direct measure of Z_{eff}(S) is the energy position of the S $1s \rightarrow 4p$ excitation or often the most intense 'white-line' feature. A second-order relationship was established to describe the relationship of the rising-edge inflection point and thus Z_{eff}(S), and the free ligand-based transition dipole integral (I^{L}) according to equations (2) and (3); see Fig. 1. We wish to emphasize that I^{L} does not always correspond to the transition dipole integral of S-ligand salts, since the cations can have non-negligible covalent interactions with the S-donor ligand. This is most clearly visible for the Li^+ salts of thiolates (Queen *et al.*, 2013) and polysulfides (Pascal *et al.*, 2014; Wujcik *et al.*, 2017). S-based radicals (Kennepohl *et al.*, 2009) or completely ionic S-salts may provide a direct measure for I^{L}. The shift of the S $1s \rightarrow 4p$ excitation or the edge energy position between the free and the coordinated ligand can be used to estimate the transition dipole integral for the complex [I^{C}, equation (4)]. The correction in going from I^{L} to I^{C} as a function of Z_{eff}(S) using the rising-edge inflection point shift (ΔE_0^{L}) relative to the Na_2S spectrum and a slope parameter are given in equation (4) and shown in Fig. 1.

$$\text{Aliphatic S-ligands}\quad I^{\mathrm{L(C)}} = 0.37(\Delta E_0^{\mathrm{L}})^2 + 4.5, \qquad (2)$$

$$\text{N-conjugated S-ligands}\quad I^{\mathrm{L(N)}} = 0.37(\Delta E_0^{\mathrm{L}}) + 14.5, \qquad (3)$$

$$\text{TM-bound S-ligands}\quad I^{\mathrm{C}} = I^{\mathrm{L}} + \mathrm{slope}(E_0^{\mathrm{C}} - E_0^{\mathrm{L}});\ \text{with slope} = 3.2(\Delta E_0^{\mathrm{L}})^2 + 2.3. \qquad (4)$$

[1] The units of the integrated pre-edge intensity are technically electronvolts from the integration of spectral features, but, as commonly done in the literature, we will omit the unit in order to avoid the confusion that emerges when a theoretical value for transition dipole moment is considered.

Relevant to the current study is the different treatment of aliphatic [equation (2)] and N-conjugated [equation (3)] S-donor ligands. The blue trace in Fig. 1 connects data points for sodium maleonitrile (Na_2MNT) and sodium dithiocarbamate (NaDTC) S-ligand salts. Both salts contain conjugated N-centers with the S-absorber. The differentiation among these S-ligands was required by a comparison of electron paramagnetic resonance (EPR) spectroscopy and XAS results with respect to the S 3*p* character of the spin densities, and in the composition of unoccupied frontier molecular orbitals for complexes containing these two ligands. Given the limited number of examples available in the literature to date with data from both EPR and XAS techniques, the exact value of 10 unit shifts is yet to be correlated with a specific physical explanation, but is clearly required by the EPR data. A plausible physical rational of these empirical relationships is the enhanced fluorescence or Auger electron yields due to the presence of extensive N-based π-conjugation in both MNT and DTC ligands compared with the hydrocarbon-based S-donor ligands, such as the tetrathiocyclotetradecane (TTCTD). In addition to fundamental insights into the chemical bonding, the TU ligand with its conjugated N atoms offers an additional way to evaluate the applicability of the empirical relationships (green and blue traces in Fig. 1) connecting the $I^{L(C)}/I^{L(N)}$ to I^{C} dipole integrals through $Z_{eff}(S)$.

The S *K*-XANES-derived experimental S 3*p* character can be directly correlated with orbital compositions from ground state electronic structure calculations. For an extensive series of $[Ni(II)S_4]^{2-}$ complexes, it was found that generalized gradient approximation (GGA, Rung 2), metaGGA (Rung 3), hybrid GGA and hybrid metaGGA (Rung 4) functionals generally overestimate the covalency of TM–S(ligand) bonds for N-containing S-donor ligands (Queen *et al.*, 2013). As shown in GGA functionals for Cu^{2+} complexes (Szilagyi *et al.*, 2002), the *M*–*L* bond covalency (where *M* means metal and *L* means ligand) can be adjusted using hybrid functionals that combine localized ionic Hartree–Fock exchange with delocalized covalent density functional exchange terms. In this study, we employed a representative set of popular GGA, hybrid GGA and metaGGA functionals to gain a comprehensive theoretical view of the ground state frontier molecular orbital compositions to those derived from our S *K*-XANES measurements.

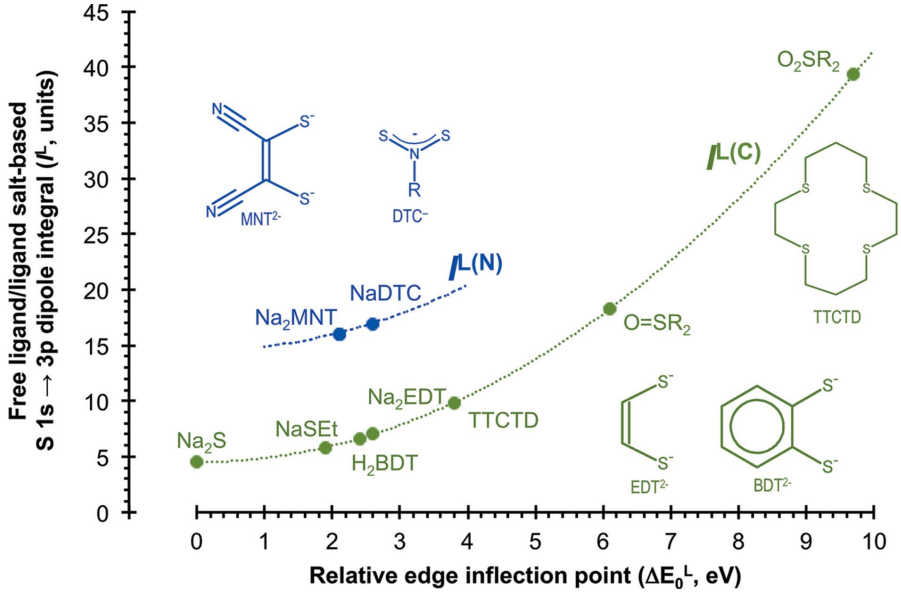

Figure 1
Correlation of relative rising-edge positions (E_0^L) referenced to the Na_2S edge-inflection point [E_0^L (sulfide) = 2471.7 eV] and the S 1*s* → 3*p* dipole integrals (I^L).

2. Materials and methods

2.1. Synthesis

TU and TM salts were purchased from Sigma–Aldrich and used without further purification. The zinc(II) TU complex, $Zn(TU)_4(NO_3)_2$, was prepared by adding 3 mmol $Zn(NO_3)_2{\cdot}6H_2O$ dissolved in 5 ml water to an aqueous solution of TU (12 mmol in 10 ml H_2O) stirring at 65°C; colorless crystals were formed in the refrigerator overnight (Vega *et al.*, 1978). Blue-green $Co(TU)_4(NO_3)_2{\cdot}H_2O$ crystals were prepared in boiling *n*-butanol, following an earlier report (Cotton *et al.*, 1964). Green nickel(II) TU crystals, $Ni(TU)_6(ClO_4)_2$, were prepared by refluxing a mixture of $Ni(ClO_4)_2{\cdot}6H_2O$ and TU (1:6 mole ratio) in absolute ethanol (Frisch *et al.*, 2009). These TM complexes were characterized by elemental analysis and/or determining their unit-cell dimensions (Spofford & Amma, 1976; Vega *et al.*, 1978).

2.2. X-ray absorption measurements

The S *K*-edge XANES spectra for the above TU complexes, the pure solid TU and its 0.5 *M* aqueous solution were measured at beamline 4–3 at Stanford Synchrotron Radiation Lightsource (SSRL), operating under storage ring conditions of 3 GeV and 500 mA current. Beamline 4-3 is a 2.0 T wiggler beamline, equipped with a liquid N_2 cooled Si(111) double-crystal monochromator and an Rh-coated harmonic rejection mirror. The energy of the incident beam was calibrated by assigning the first peak in the S *K*-edge XANES spectrum of $Na_2S_2O_3{\cdot}5H_2O$ to 2472.02 eV. S *K*-edge XANES spectra were collected in the energy range 2420–2740 eV using an unfocused 3 × 1 mm beam, in an He-purged beam path, at room temperature with a passivated implanted planar silicon (PIPS) fluorescence detector (CANBERRA). Solid samples were ground finely and dusted on sulfur-free Mylar tape. The spectra of the $Ni(DTC)_2$ and $[Ni(TTCTD)_2(ClO_4)_2]$ complexes were taken from the supplementary information of the work by Queen *et al.* (2013).

2.3. Data fitting

All spectra were background-subtracted and normalized using the *Automated Data Reduction Protocol* (*ADRP*) developed by Gardenghi (2011). The normalized S *K*-edge spectra (Fig. 2) were modeled using *Peak Fit* (version 4.12, SeaSolve) to obtain pre-edge peak intensities (*D*) from peak amplitudes (*A*), energy positions (E_0) and line-widths (*lw*). All transitions were modeled with a 'Gaussian–Lorentzian Sum Amplitude' function as defined in equation (5),

$$D = A\left[\frac{\frac{(\mathrm{G{:}L})(\ln 2)^{1/2}}{lw(\pi)^{1/2}}\exp\left(-4\ln 2\left(\frac{E-E_0}{lw}\right)^2\right)+\frac{1-(\mathrm{G{:}L})}{\pi lw\left[1+4\left(\frac{E-E_0}{lw}\right)^2\right]}}{\frac{(\mathrm{G{:}L})(\ln 2)^{1/2}}{lw(\pi)^{1/2}}+\frac{1-(\mathrm{G{:}L})}{\pi lw}}\right]. \quad (5)$$

The Gaussian/Lorentzian ratio (G:L) was maintained at a value of 0.5 for well resolved excitations involving a single or degenerate double electron hole(s). This corresponds to a commonly used pseudo-Voigt line shape. The shared line-widths (*lw*) and G:L mixing ratios were allowed to deviate from the optimal values of 1.0–1.4 eV and 0.5, respectively. The ionization threshold also referred to as edge jump was modeled with a 'Lorentzian cumulative' step function as defined in equation (6),

$$D = \frac{A}{\pi}\left[\tan^{-1}\left(\frac{E-E_0}{lw}\right)+\frac{\pi}{2}\right], \quad (6)$$

where *A* is the edge jump height set to 1.0 for a normalized spectrum, E_0 is the absorber ionization energy and *lw* is the line-width or the slope of the edge jump. Fits were obtained stepwise by allowing for the line-widths, amplitudes and, lastly, the energy positions to vary. The final spectral models were obtained by relaxing all parameters except the G:L mixing ratio.

In order to obtain meaningful error bars for the fitting procedure, the $[Ni(TU)_6]^{2+}$ and $[Co(TU)_4]^{2+}$ S *K*-XANES spectra were also baseline- and background-corrected using the free TU and $[Zn(TU)_4]^{2+}$ spectra. The spectra of the free ligand and Zn complex in the energy range 2460–2480 eV were converted into a single analytical function (user-defined function, UDF in *PeakFit*) that describe S $1s \rightarrow$ C—S σ^*/π^* and $1s \rightarrow 4p$ features and the edge jump with the sum of individual functions shown in equations (5) and (6), respectively. When using the UDFs for fitting the spectra of the $[Ni(TU)_6]^{2+}$ or $[Co(TU)_4]^{2+}$ complexes, the energy position and intensity of the UDF were allowed to vary with shift and scale applied to all components uniformly. Furthermore, additional fits were guided by the IR study of the $[Ni(TU)_6]^{2+}$ complex (El-Bahy *et al.*, 2003) with regards to change in the valence bond picture of TU upon coordination to the nickel(II) ion. To model the change in the valence bond picture, we varied the integrated intensity ratio of the C—S π^* to C—S σ^* peaks from 0.2 to 0.4. However, these gave at most 4% variation in pre-edge intensity, which translates to a negligible (<1%) change in the S 3*p* orbital characters.

2.4. Electronic structure calculations

Electronic structure calculations of free TU and its S-protonated form as an extreme Brønsted acid representation for the TU's thiol form, mimicking the Lewis acidity of TM ion in $[Co(TU)_4]^{2+}$, $[Zn(TU)_4]^{2+}$ and $[Ni(TU)_6]^{2+}$ complexes, were performed using the *Gaussian09* quantum chemical package (Frisch *et al.*, 2009). The main electronic structure feature was the TM and ligand contributions to the unoccupied frontier molecular orbitals that we probed by S *K*-XANES. Since the complexes are charged, we carried out all calculations using the polarizable continuum model (PCM) (Cossi *et al.*, 1996; Mennucci & Tomasi, 1997; Miertuš *et al.*, 1981; Pascual-ahuir *et*

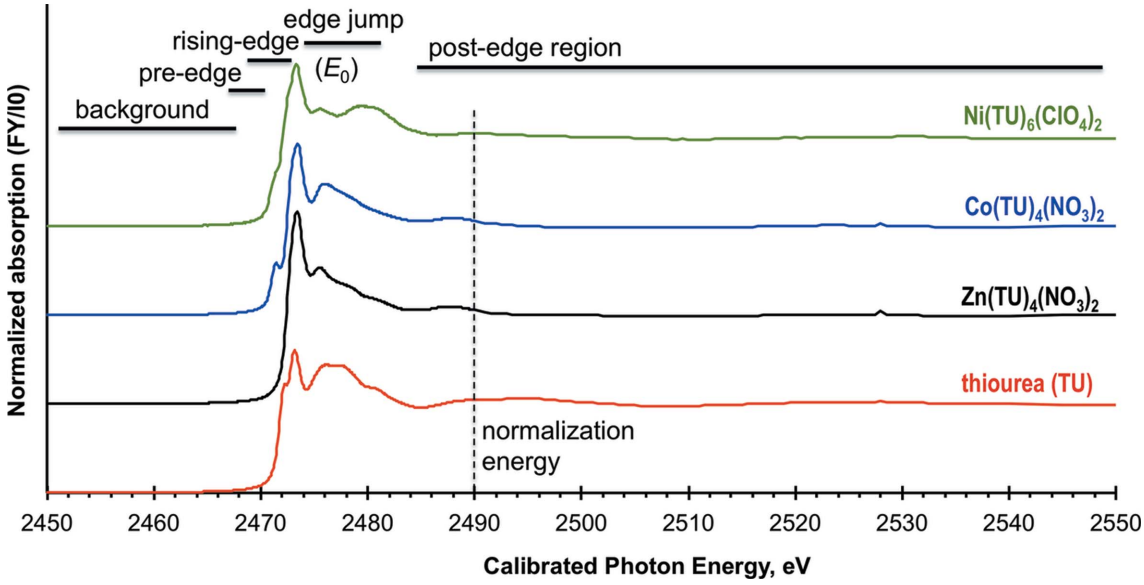

Figure 2
Overview of the full range S *K*-edge XANES spectra of pure TU and its Zn^{2+}, Co^{2+} and Ni^{2+} complexes as a demonstration of spectral quality and normalization procedure.

al., 1994; Tomasi *et al.*, 2005) with solvent parameters for acetonitrile with ϵ = 35.5 [PCM(CH_3CN)] to mitigate distortions to the electronic structure due to *in vacuo* modeling. High-quality crystal structures of free TU ligand, $[Zn(TU)_4](NO_3)_2$, $[Co(TU)_4](NO_3)_2{\cdot}H_2O$ and $[Ni(TU)_6]Br_2$ complexes (Kutoglu *et al.*, 1982; Spofford & Amma, 1976; Vega *et al.*, 1978; Weininger *et al.*, 1969) were used without structural optimization for electronic structure analysis, since even the positions of the hydrogen atoms were refined experimentally. To be conceptually correct with respect to theoretically predicted IR spectra that provide independent validation of the XANES analysis (see supporting information), the geometries of the complexes had to be optimized. We used the BP86 functional (Becke, 1988; Perdew, 1986) and def2-TZVP basis set (Weigend & Ahlrichs, 2005) in the acetonitrile PCM environment [BP86/def2-TZVP/PCM(CH_3CN)]. Frequency calculations were performed on the stationary geometries without any imaginary normal modes.

The BP86 (Becke, 1988; Perdew, 1986), TPSS (Tao *et al.*, 2003) and B3LYP (Lee *et al.*, 1988; Becke, 1993) functionals were chosen as representative examples for the GGA (Rung 2), metaGGA (Rung 3) and hybrid GGA (Rung 4) rungs of Perdew's ladder of functionals, respectively (Staroverov *et al.*, 2004; Perdew *et al.*, 2009). We chose the def2-TZVP (Weigend & Ahlrichs, 2005) basis set from the EMSL Gaussian Basis Set Exchange (Feller, 1996; Schuchardt *et al.*, 2007), which was shown to be saturated with respect to the electronic structure for Ni^{2+} complexes (Queen *et al.*, 2013). The total sulfur compositions of the unoccupied frontier molecular orbitals corresponding to the TM–S(ligand) bonds were obtained from Bader's 'Atoms in Molecule' (AIM) population analysis (Bader, 1985, 2010; Cortesguzman & Bader, 2005) using the *AIMAll* program (Keith, 2011). Differential atomic orbital contributions were obtained from Weinhold's natural population analysis (NPA) (Foster & Weinhold, 1980) using valence electron configurations for M^{2+} [3*d*4*s*4*p*] and for S [3*s*3*p*3*d*].

Equilibrium structures of the studied complexes and the free TU ligand, and related vibrational analysis results are shown in Figs. S1–S3 and Table S2 of the supporting information that further aid the interpretation of the XAS spectra with respect to the shift in electronic structure from the thione to thiolate form upon coordination to a TM cation.

3. Results and discussions

In order to extract ground state frontier molecular orbital compositions from S *K*-XANES pre-edge and rising-edge features, we first assigned the spectral features and estimated the ionization threshold or edge positions for the free TU ligand and the Ni^{2+} and Co^{2+} complexes. This allowed for the estimation of transition dipole integrals for the free (I^L) and the coordinated ligands (I^C) using the relationships in equations (2)–(4) and in Fig. 1. The formal oxidation state of the S absorbers in the TU ligand can be placed on a continuum between dithiocarbamate and thioether ligands. The modeling of the pre-edge and rising-edge spectral features gave us with the normalized pre-edge intensities (D_0) which, when input into equation (1), provides the S 3*p* contribution (α^2) to the covalent TM^{2+}–S(TU) bonding.

3.1. Free ligand transition dipole integral (I^L) for TU

The XANES region of the S *K*-edge spectra for TU is compared with sodium dithiocarbamate (NaDTC) and tetrathiocyclotetradecane (TTCTD) in Fig. 3(*a*) along with the first [Fig. 3(*b*)] and second derivatives [Fig. 3(*c*)]. Within the rising-edge region of 2474–2476 eV, a gradual shift in the S 1*s* → 4*p* feature/edge position can be observed in the order of Na(DTC) (2474.3 eV), TU (2474.6 eV) and then TTCTD

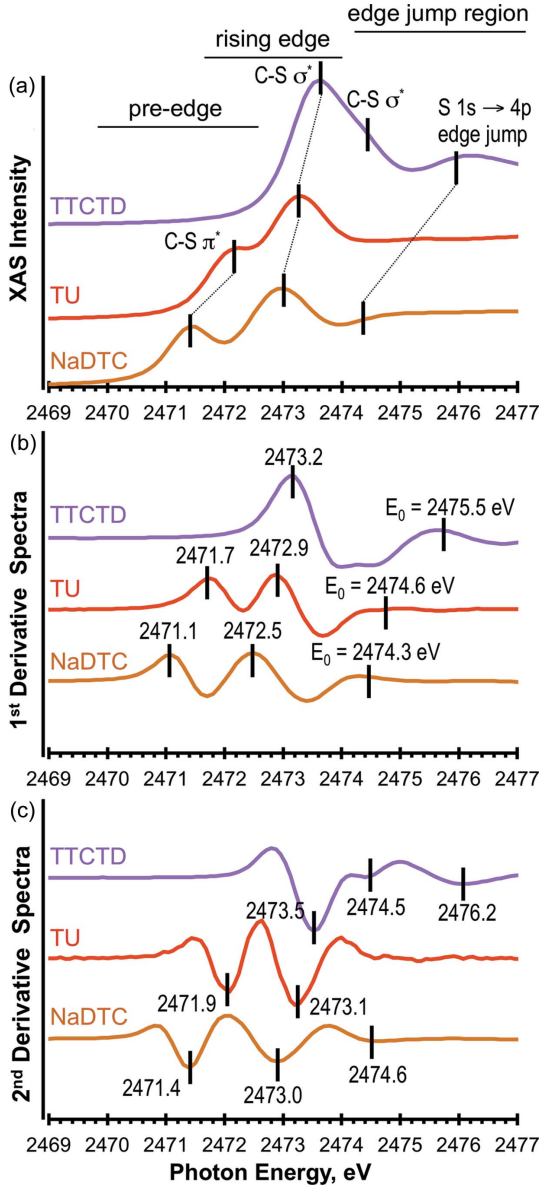

Figure 3
(*a*) S *K*-XANES spectra of the free TTCTD, TU and sodium salt of NaDTC, (*b*) first- and (*c*) second-derivative spectra (all resolved peaks are marked based on the second-derivative minimum positions). The white-line features for free ligands are formed by the C—S σ* transitions originating from varied chemical environments.

Table 1
Summary of parameters used estimating free ligand dipole integrals (I^{L}) for NaDTC, TU and TTCTD ligands.

Ligands	E_0 (eV)†	E_0^{L} (eV) ‡	$I^{L(C)}$ (units)	$I^{L(N)}$ (units)	Slope
DTC^{-}	2474.3	2.6	NA	16.9	23.9
TU	2474.6	2.9	7.6	17.6	29.2
TTCTD	2475.5	3.8	9.8	NA	48.5

† From first-derivative spectra in Fig. 3(*b*). ‡ Relative value to Na_2S at 2471.7 eV.

(2475.5 eV). Historically (Solomon *et al.*, 2005), the edge position (E_0) is assigned to its first inflection point, *i.e.* the first maximum of the first derivative; however, the greatly varied covalent bonding involving the S center(s) in the above three S-donor ligands prohibits this approximation due to the presence of overlapping spectral features from π- and σ-bonding. Using trends in the energy positions for the entire series of S-donor ligands from a systematic comparison (Queen *et al.*, 2013), the edge position can be assigned for the first inflection point after the last resolved rising-edge feature/white line at 2474.6 ± 0.5 eV. The considerable uncertainty in the edge positions is due to the limited resolution of the S 4*p*/edge jump feature for the TU free ligand above the white line at 2473.5 eV. Using a molecular orbital description of the free ligand (see below), the S 1*s* → C—S π*, 1*s* → C—S σ* transitions can be assigned as indicated in Fig. 3(*a*).

The relative rising-edge position is 2.9 eV in TU, which gives a free-ligand dipole integral of 17.6 ± 0.6 units from equation (3) or Fig. 1. This is 0.7 units greater than the $I^{L(N)}$ of DTC (16.9 units). In contrast, the $I^{L(C)}$ value is 7.6 ± 0.6 units, which is 2.2 units less than that of TTCTD (9.8 units) when using the relationship for the hydrocarbon-only S-ligands in equation (2). The high and low values of I^{L}(TU) can be considered as chemically reasonable since the free TU has a neutral formally thione sulfur, but it is also involved in π-conjugation with the NH_2 groups. Furthermore, the edge position (E_0) determines the slope parameter used to account for the change of Z_{eff}(S) in going from the free to the coordinated ligand given by equation (4). For the free TU ligand, the slope parameter is 29.2, which is also reasonable when compared with DTC at 23.9 and TTCTD at 48.5. Table 1 summarizes the relevant free-ligand-based values for NaDTC, TU and TTCTD. The correct free ligand transition dipole integral cannot be simply defined solely based on free-TU spectra without taking into account the pre-edge intensities of TU complexes.

3.2. Transition dipole integral (I^{C}) for coordinated sulfur in $[Ni(TU)_6]^{2+}$ and $[Co(TU)_4]^{2+}$

The S *K*-XANES spectra for $[Zn(TU)_4]^{2+}$, $[Co(TU)_4]^{2+}$ and $[Ni(TU)_6]^{2+}$ are compared with the previously analyzed spectra of $Ni(DTC)_2$ and $[Ni(TTCTD)]^{2+}$ complexes along with their first and second derivatives in Fig. 4 (Queen *et al.*, 2013). The pre-edge features at 2471.2 eV and 2471.1 eV for $[Co(TU)_4]^{2+}$ and $[Ni(TU)_6]^{2+}$ form Fig. 4(*c*), respectively, are due to the S 3*p* character of electron holes in the Co/Ni—S σ*/π* orbitals. This feature is absent in $[Zn(TU)_4]^{2+}$ because of the filled 3*d* manifold. The rising-edge positions (estimated from S 1*s* → C—S π* excitations) of all TM^{2+}–TU complexes shift by 0.4–0.8 eV to higher energy [Fig. 4(*b*), Ni^{2+}: 2472.1, Co^{2+} and Zn^{2+}: 2472.5 eV] relative to free TU [Fig. 3(*b*), 2471.7 eV], which parallels the estimated edge position shifts of 0.4–0.9 eV [Fig. 4(*b*), Ni: 2475.1 eV, Co: 2475.2 eV, Zn: 2475.0 eV *versus* Fig. 3(*b*), TU: 2474.6 eV]. The significant chemical shifts are a clear indication of shifting the dominance of resonance structures along the continuum as illustrated in Scheme 1.

The edge position (E_0) for $[Ni(TU)_6]^{2+}$, although better resolved than in the free-TU spectrum [compare red trace in

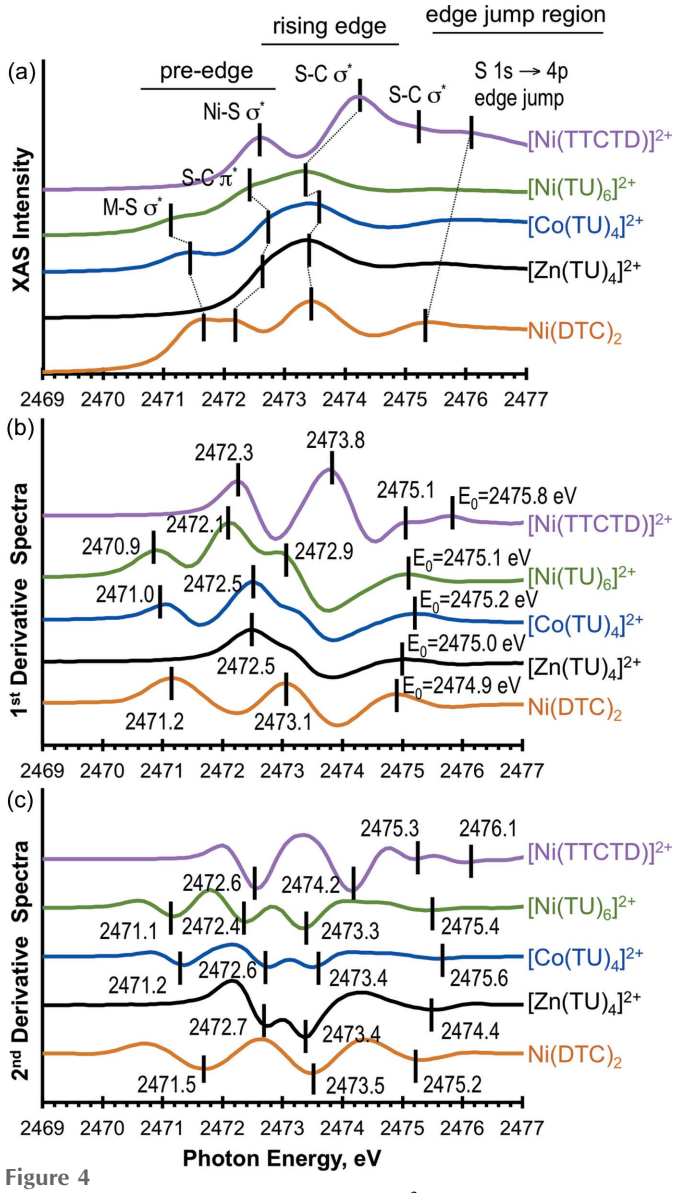

Figure 4
(*a*) S *K*-XANES spectra of reference Ni^{2+} coordination compounds ($[Ni(TTCTD)]^{2+}$ and {$[Ni(DTC)_2]$}, and the TU complexes of Ni^{2+}, Co^{2+} and Zn^{2+}; (*b*) first- and (*c*) second-derivative spectra (all resolved peaks are marked based on the second-derivative minimum positions). The white-line features for the TU complexes are formed by the C—S σ* transitions originating from varied chemical environments.

Fig. 3(*b*) and green trace in Fig. 4(*b*)], cannot be assigned unambiguously without considering the spectra of other complexes. The spectral features of $Ni(DTC)_2$ and $[Ni(TTCTD)]^{2+}$ in the edge/post-edge region [thin slanted line in Fig. 4(*a*)] suggest an edge position of 2475.1 ± 0.3 eV for $[Ni(TU)_6]^{2+}$, which is 0.5 eV greater than the edge position of the free TU ligand [Fig. 3(*b*), 2474.6 eV]. The shift is the direct measure of the increase in Z_{eff}(S) of TU upon coordination to the Ni^{2+} ion.

Applying equation (4) for connecting $I^{L(N)}$(TU) and $I^{C}([Ni(TU)_6]^{2+})$, a S 1*s* → 3*p* transition dipole integral value of 32.2 units can be derived for $[Ni(TU_6)]^{2+}$. This is a reasonable value when compared with I^{C} for $Ni(DTC)_2$ (31.2 units). When the lower value of $I^{L(C)}$(TU) is considered, the $I^{C}\{[Ni(TU)_6]^{2+}\}$ dipole integral is 22.2 units, which is again reasonable when compared with $[Ni(TTCTD)]^{2+}$ (23.3 units), respectively. The edge position for $[Co(TU)_4]^{2+}$ (E_0 = 2475.2 ± 0.3 eV) is shifted by +0.6 eV relative to free TU, which corresponds to a dipole integral I^{C} for the Co^{2+} complex of 25.1 and 35.1 units when the free ligand dipole integrals of $I^{L(C)}$ and $I^{L(N)}$ are considered, respectively. The significant differences in the estimated values of free (I^{L}) and coordinated (I^{C}) ligand dipole moments illustrate the challenges in modeling the ground-state electronic structure from XANES features as well as rationalizes the need for independent spectroscopic techniques (EPR, ENDOR, ESEEM) or theoretical methods (electronic structure calculation) to tighten the correlation among pre-edge intensities and unoccupied orbital compositions.

3.3. Determination of normalized pre-edge intensity (D_0) for the free ligand

Following the detailed analyses of ligands DTC and TTCTD (Queen *et al.*, 2013), Fig. 5 shows representative pseudo-Voigt line fits to the S 1*s* → C—S π^*, C—S σ^*, S 4*p* and the S 1*s* ionization threshold (edge jump) for the S *K*-edge XANES spectrum. The well resolved S 1*s* → C—S π^* pre-edge feature is located at 2472.1 eV with 1.33 unit intensity, and the rising-edge C—S σ^* transition at 2473.3 eV with D_0 = 2.92 unit intensity. Given that TU has formally a σ- and a π-bond, the approximate double peak intensity for the latter should correspond to considerably larger S character in the antibonding C—S σ^* orbital. However, as discussed later during the electronic structure analysis, the second feature cannot be purely assigned to C—S σ^*-based excitations. Using the free TU ligand dipole integral $I^{L(C)}$ (7.6 units) or $I^{L(N)}$ (17.6 units) (Table 1) and equation (1), the S 3*p* orbital character of the C—S π^* feature can be estimated to be $0.26e^-$ and $0.11e^-$ per hole, respectively. These values appear to be too small when considering the difference between Z_{eff}(S) and Z_{eff}(C) which defines the antibonding, unoccupied molecular orbitals to be dominantly S-based; however, as shown later, the N-conjugation mixes a significant amount of N 2*s*/2*p* character with the C 2*s*/2*p* and S 3*p*-based unoccupied, frontier molecular orbitals.

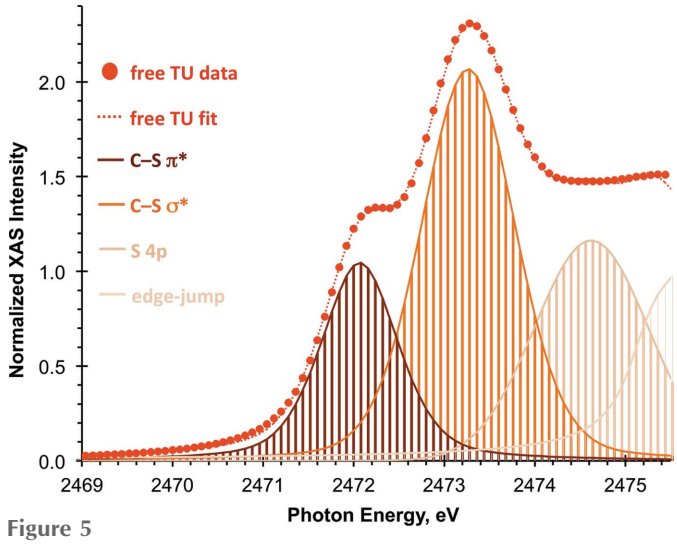

Figure 5
Pseudo-Voigt line fits to the S *K*-edge XANES of free TU with S 1*s* → C—S π^*, C—S σ^*, S 4*p* and an edge-jump fit at the S 1*s* ionization threshold.

3.4. Determination of normalized pre-edge intensity (D_0) for coordinated ligands

As discussed earlier (Queen *et al.*, 2013), the Ni–S bond covalencies in $[Ni(DTC)_2]$ and $[Ni(TTCTD)]^{2+}$ were determined to be $0.31e^-$ and $0.39e^-$ per hole, respectively, corresponding to highly covalent bonding. Fig. 6 shows representative fits to the spectra of (*a*) $[Zn(TU)_4]^{2+}$, (*b*) $[Co(TU)_4]^{2+}$ and (*c*) $[Ni(TU)_6]^{2+}$ after subtracting the free-TU spectrum shifted by +0.48 eV, +0.44 eV and +0.31 eV, respectively, for a chemically reasonable background correction and rising-edge subtraction. All the spectra of the complexes contain C—S π^* and C—S σ^* features which are poorly fit by the free-TU ligand spectrum, as can be seen from the spectral range above 2472 eV. This is the direct experimental indication that the electronic structure of the coordinated and free TU ligands changes upon coordination as also suggested by the IR spectra of the complexes (Yamaguchi *et al.*, 1958; Kumler & Fohlen, 1942; El-Bahy *et al.*, 2003). In addition, the S *K*-XANES spectra of $[Co(TU)_4]^{2+}$ and $[Ni(TU)_6]^{2+}$ have a well resolved pre-edge feature due to the S 1*s* → TM–S σ/π^* excitation [blue and green peaks below 2472 eV, Figs. 6(*b*) and 6(*c*)]. This pre-edge feature is absent in $[Zn(TU)_4]^{2+}$ due to the Zn^{2+} ion $3d^{10}$ electron configuration. The normalized integrated pre-edge intensities (D_0) for the $[Co(TU)_4]^{2+}$ and $[Ni(TU)_6]^{2+}$ complexes were found to be comparable with values of 0.54 units and 0.59 units, respectively, despite the different number of S-absorbers (N) and electron holes (h).

In order to investigate improvements to the fits in Fig. 6 along the rising-edge region, the C—S π^* feature was separated from the analytical (UDF) free-TU ligand spectrum and fitted with a separate pseudo-Voigt line as shown in Fig. 7 for $[Zn(TU)_4]^{2+}$, $[Co(TU)_4]^{2+}$ and $[Ni(TU)_6]^{2+}$. This approach allows for direct monitoring of the structurally versatile nature of the TU ligand in which the thione (C═S π^*) character of the S absorber gradually shifts toward a thiolate (C–S σ^*) character.

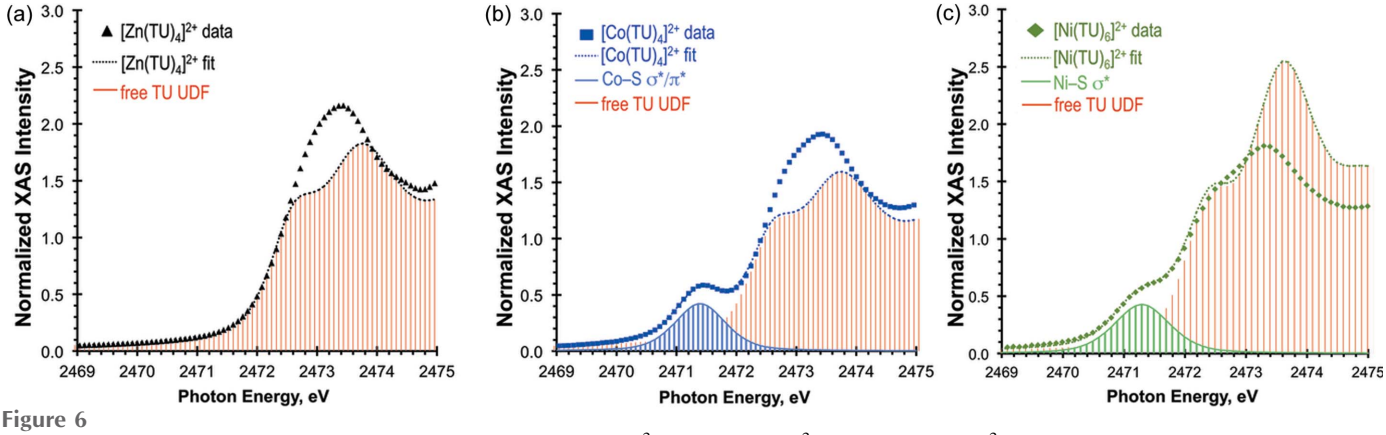

Figure 6
Representative fits to the S *K*-edge XANES spectra of (*a*) $[Zn(TU)_4]^{2+}$, (*b*) $[Co(TU)_4]^{2+}$ and (*c*) $[Ni(TU)_6]^{2+}$ using the shifted (+0.48 eV +0.44 eV and +0.31 eV, respectively) analytical free-TU spectrum UDF for background correction and rising-edge subtraction.

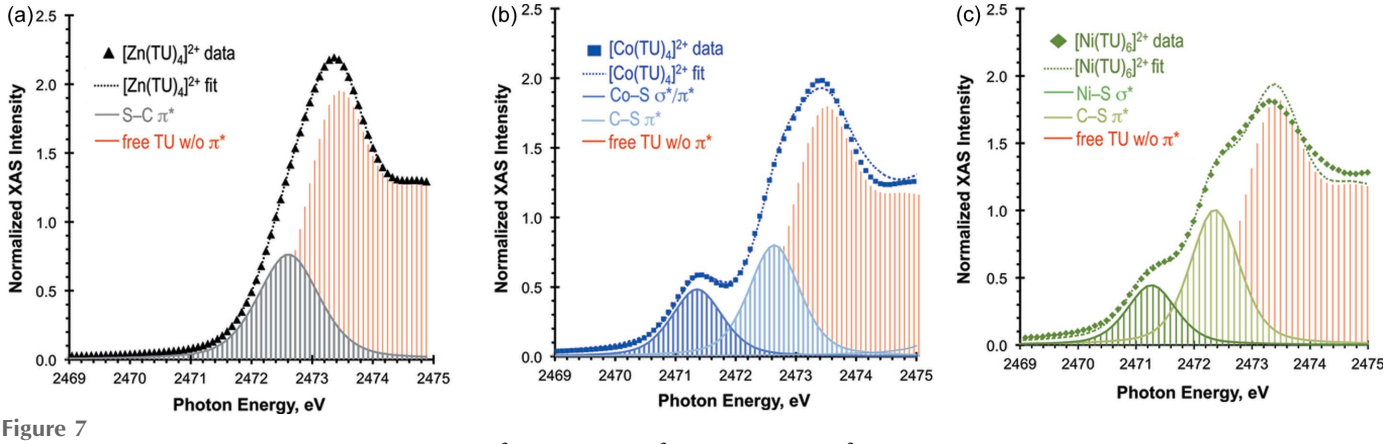

Figure 7
Fits to the S *K*-edge XANES spectra of (*a*) $[Zn(TU)_4]^{2+}$, (*b*) $[Co(TU)_4]^{2+}$ and (*c*) $[Ni(TU)_6]^{2+}$ using the free-ligand spectrum UDF without the S 1*s* → C—S π^* feature.

The fits in Fig. 7 with two linked pseudo-Voigt lines for the S 1*s* → TM–S σ^*/π^* and C–S π^* transitions gave D_0 values of 0.61 units and 0.57 units for the pre-edge feature/TM–S σ/π^* bonding in $[Co(TU)_4]^{2+}$ and $[Ni(TU)_6]^{2+}$, respectively. Notably, the S 1*s* → C—S π^* excitation features show comparable intensities for the $[Zn(TU)_4]^{2+}$ and $[Co(TU)_4]^{2+}$ complexes (1.08 units and 1.02 units, respectively). However, it is significantly different (1.22 units) for $[Ni(TU)_6]^{2+}$ due to the greater number of TU ligands and the expected reduced thiolate *versus* the thione character. This can also be correlated with the importance of thione and thiolate resonance structures of TU (Scheme 1). The Ni–S(TU) coordination is based on a better metal–ligand overlap; however, the manifestation of a greater thiolate character is hindered by the greater number of TU ligands in Ni^{2+} *versus* Co^{2+} complexes.

The near-identical TM–S(TU) pre-edge intensities within the error of XAS data collection and analysis (Giles *et al.*, 2011) do not correspond to identical S 3*p* contributions, since the Co^{2+} complex has three *d*-electron holes and four absorbers, while the Ni^{2+} complex has two holes for six absorbers. The renormalized intensity values are 0.8 units and 1.7 units per hole for $[Co(TU)_4]^{2+}$ and $[Ni(TU)_6]^{2+}$, respectively, which now clearly indicate a *ca* double TM–S bond covalency in the octahedral Ni^{2+} *versus* tetrahedral Co^{2+} complex, as expected from the difference in the number of ligands and the efficiency of the *M–L* overlap between the two coordination environments.

Numerous reasonable fits can be achieved by varying the relative contributions of the TM–S σ^*/π^* peak as a function of the C—S π^*/C—S σ^* peaks. This leads to a spectral modeling uncertainty that we evaluated by varying the ratio of these two features from 0.4 (free ligand, Fig. 6) to 0.2 (coordinated complex, Fig. 7) as shown in Fig. 8 for the example of the $[Ni(TU)_6]^{2+}$ complex, while all resolved features were allowed to vary independently. It is noteworthy that the estimated rising-edge position in Table 1 varies from the S 1*s* → 4*p*/edge-jump positions from the fits in Fig. 8. Furthermore, the fit to the S 4*p* transition was allowed to float, which resulted in a *ca* 0.4 eV shift to lower energy relative to the edge-jump. The differences in experimental energy positions and those from modeling may require a recursive iterative spectral modeling that we did not carry out here due to the anticipated modest variation in the dipole integral values. This simplification is rationalized by the less than 2% variation in the Ni—S σ^*-based integrated pre-edge intensities (D_0) of 0.50–0.53 units. Therefore, we can obtain a reasonable fit for the pre-edge

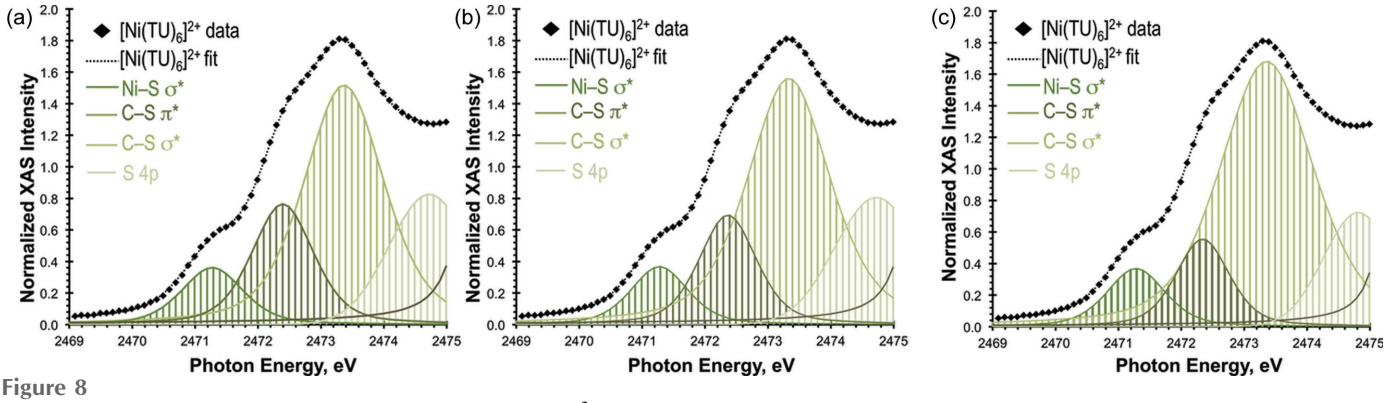

Figure 8
Comparative fits to the S *K*-edge XANES spectra of $[Ni(TU)_6]^{2+}$ with pseudo-Voigt lines for the S 1*s* → C–S π*, C–S σ*, S 4*p* transitions and an edge-jump for the S 1*s* ionization, when the ratio of C–S π* to C–S σ* intensity was fixed at (*a*) 0.4, (*b*) 0.3 and (*c*) 0.2.

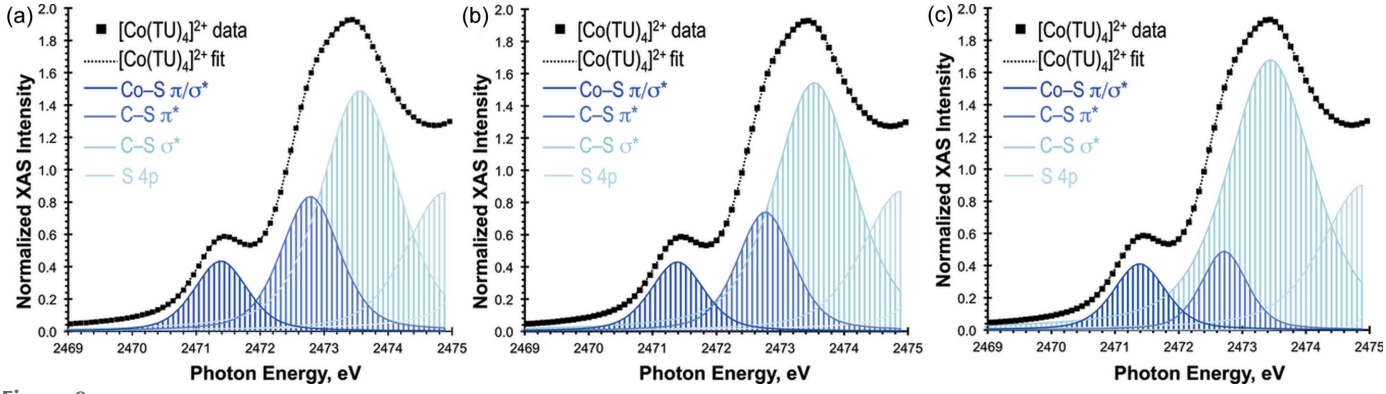

Figure 9
Comparative fits to the S *K*-edge XANES spectra of $[Co(TU)_4]^{2+}$ with pseudo-Voigt lines for the S 1*s* → C–S π*, C–S σ*, S 4*p* transitions and an edge-jump for the S 1*s* ionization, when the ratio of C–S π* to C–S σ* intensity was fixed at (*a*) 0.4, (*b*) 0.3 and (*c*) 0.2.

intensities when the change in the C—S π* spectral features is fit independently from the envelope of excitations that make up the rest of the rising-edge region.

Fig. 9 summarizes a complementary analysis for the Co^{2+} complexes with systematically varied ratios of the second and third resolved rising-edge features. The unconstrained fit to the pre-edge and rising-edge features with separate Co—S π/σ*, C—S π*, C—S σ*, S 4*p* features and edge position of $[Co(TU)_4]^{2+}$ resulted in a well resolved Co—S π/σ*-based transition of 0.55 unit intensity without significant variation. Furthermore, this is almost identical to the result obtained for the free-ligand-corrected fit in Fig. 6(*b*), and slightly less than the fit shown in Fig. 7(*b*) with a separate C—S π* feature.

It is insightful to compare the spectra of the two tetrahedral species. The $[Zn(TU)_4]^{2+}$ complex with a $3d^{10}$ filled *d*-manifold has only limited 4*s*/4*p* orbital-based covalent bonding. Thus, the rising-edge features in the spectrum of $[Zn(TU)_4]^{2+}$ represent the overall effect of the dominant ionic bonding between the Zn^{2+} ion and the TU ligands. Therefore, a representative fit to the spectrum of $[Zn(TU)_4]^{2+}$ [Fig. 10(*a*)] can be directly used for background and rising-edge correction for the isostructural $[Co(TU)_4]^{2+}$ complex. Similarly to the free ligand, an analytical function was created for the $[Zn(TU)_4]^{2+}$ spectrum, which was then used to obtain the fit shown in Fig. 10(*b*). This fit can be considered as the most accurate estimate of the Co–S(TU) 3*d*-orbital based covalent bonding with practically no residuals within the rising-edge region. The first pre-edge feature in Fig. 10(*b*) corresponds to a 0.53 unit integrated pre-edge intensity.

The final integrated pre-edge intensities corresponding to the S 1*s* → Co—S π/σ* and Ni—S σ* excitations were obtained by averaging the normalized pre-edge intensities (D_0) from the compilation of fitting results presented in Table S1 of the supporting information. The free-TU ligand based fits shown in Fig. 6 were excluded due to inferior fitting of the C—S σ* features compared with other fits. The resulting average normalized Co—S π/σ* and Ni—S σ* intensities are 0.56 ± 0.04 units and 0.53 ± 0.03 units, respectively. In order to obtain the experimental TM–*L* bond covalency values, we need to evaluate the different values for S 1*s* → TM 3*d*/S 3*p* empirical transition dipole integrals as defined by equations (2) and (3).

3.5. Determination of experimental TM–S(TU) bond covalency

Table 2 condenses all relevant fitting parameters from Table S1 for the ligand and complex S *K*-edge XANES spectra used to determine the S 3*p* character of the experimentally probed 3*d*-based orbitals as the measure of TM–S covalent

Table 2
Parameters used to obtain experimental S 3*p* character for TU complexes of Co^{2+} and Ni^{2+}.

	D_0 (unit)	E_0^L (eV)	I^L (unit)		E_0^L (eV)	Slope	I^C (unit)	S 3*p* (e^- per hole)
$[Ni(TU)_6]^{2+}$	0.53 ± 0.3	2474.6 ± 0.5	C-based	7.6 ± 0.8	0.5	29.2	22.2	0.21 ± 0.05
			N-based	17.6 ± 0.8			32.2	0.15 ± 0.05
$[Co(TU)_4]^{2+}$	0.56 ± 0.4		C-based	7.6 ± 0.8	0.6		25.1	0.09 ± 0.04
			N-based	17.6 ± 0.8			35.1	0.06 ± 0.04

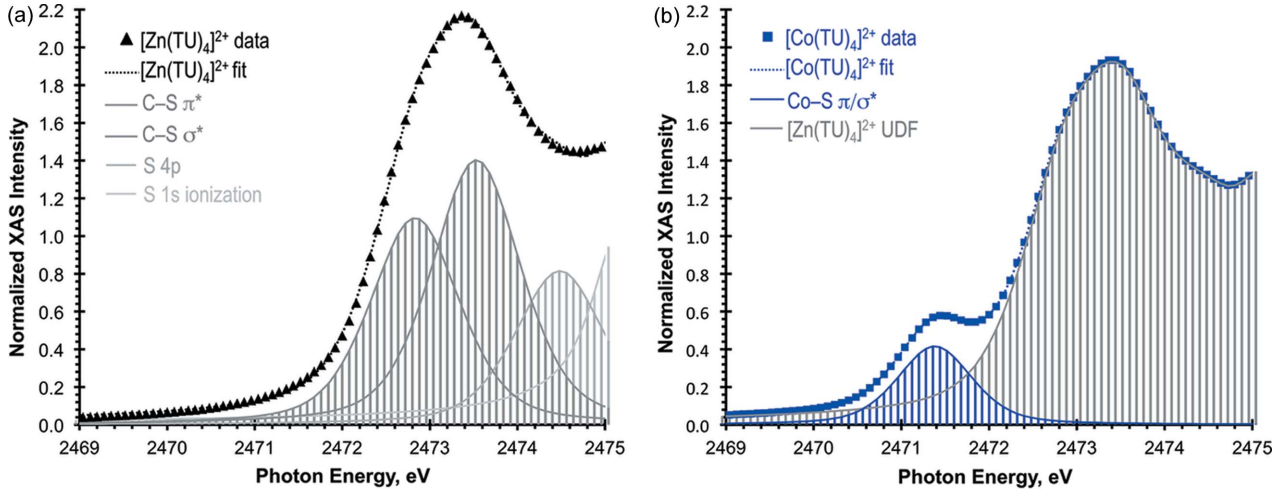

Figure 10
S *K*-edge XANES spectra of (*a*) $[Zn(TU)_4]^{2+}$ and (*b*) $[Co(TU)_4]^{2+}$. The latter was fit using the analytical UDF containing the four individual spectral fits from (*a*) (gray traces).

bonding from equation (1) and the transition dipole relationships from equations (2)–(4) as shown in Fig. 1.

As described above, the numerically comparable pre-edge intensities (D_0) will result in different S 3*p* contributions due to the different number of S absorbers and electron holes in the 3*d*-manifold. The covalency of Ni—S(TU) bonds is more than twice that of Co—S(TU) as a result of an approximate octahedral coordination geometry with better TM–*L* overlap than the approximate tetrahedral geometry for the Co^{2+} complex. The at most 21% covalency per electron hole corresponds to a normal bonding scheme (Szilagyi, 2009), where the TM 3*d* orbitals are at a higher energy relative to the S-donor 3*p* orbitals with a modest TM–*L* overlap. In other words, the antibonding TM–*L* orbitals are predominantly metal-based. Such electronic structure features differentiate these TU complexes as being structurally versatile due to various resonance structures that are at play *versus* the redox non-innocence observed when intramolecular redox chemistry occurs as a result of complex formation. The Co–S(TU) bond shows a small variation (3%) in covalency as a function of the transition dipole integral (I^C), thus it cannot be used to critically evaluate the preference of using a hydrocarbon ($I^{L(C)}$) or N-conjugated ($I^{L(N)}$) free-ligand dipole integrals. However, the ∼6% difference in Ni–S(TU) bond covalency is already significant for evaluating the adequacy of using a larger transition dipole integral ($I^{C(N)}$) due to the N-conjugated S-ligand structure.

3.6. Calculated ground state electronic structure

The crystal structure of the free TU was used to derive the ground state molecular orbital diagram as shown in Fig. 11(*a*) at the BP86/def2-TZVP/PCM(CH_3CN) level of theory. The highest occupied molecular orbital (HOMO) is the in-plane S lone pair with a small N character. This is going to be the dominant σ-donor orbital that forms the covalent TM–S bond. The lowest unoccupied molecular orbital (LUMO) is an out-of-plane C—S π* with significant conjugation into the N centers. The HOMO and LUMO compositions indicate the preference for the use of the $I^{L(N)}$ transition dipole integral. One of the in-plane N—H antibonding orbitals forms LUMO+1, which will not be detected by S *K*-edge XANES experiments due to its less than 1% sulfur contribution. The next experimentally important orbital is the C—S σ with again significant N and C character. The orbital ordering in Fig. 11(*a*) supports the S *K*-XANES assignments in Fig. 3 for the free TU ligand.

The AIM population analysis for the atomic orbital composition in the free TU ligand gives a delocalized C—S π*-based LUMO with only $0.26e^-$ per hole total S character. The LUMO+2 or C—S σ* orbital has $0.32e^-$ per hole S contribution. The ratio of the S character in the C—S π* and σ* orbitals (0.19) support the previous assumption that the intense, higher energy feature of the rising-edge cannot be solely assigned to the C—S σ* transition as shown in Fig. 5.

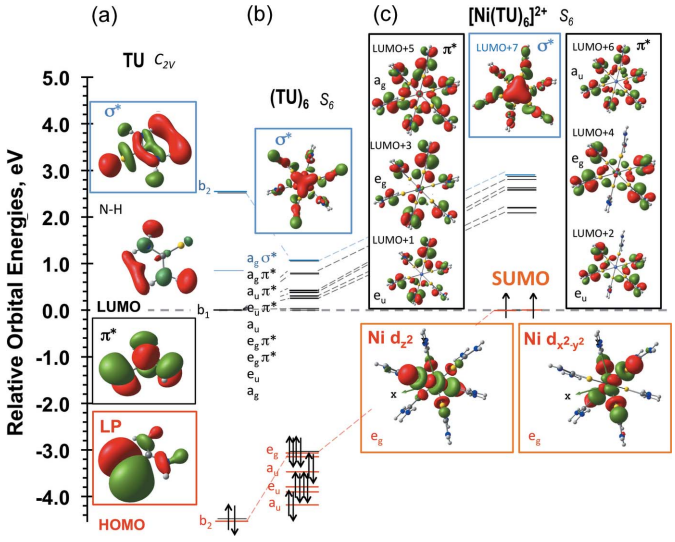

Figure 11
Ground state MO diagram calculated at the BP86/def2-TZVP/PCM(CH_3CN) level for the symmetrized C_{2v} X-ray structure of (*a*) free TU, (*b*) S_6 symmetrized hexamer $(TU)_6$ of free ligands without a central metal ion and (*c*) $[Ni(TU)_6]^{2+}$ complex with S_6 symmetry.

This ratio can also be taken as a quantitative description for the state of the resonance structures between the thione and the thiolate form (Scheme 1). The latter form should have no spectral feature for the C—S π^* transition. Using the dipole expression of equation (1), the AIM-calculated S orbital contributions and the D_0 values for the C—S π^* transition, a free ligand integral (I^{L}) of 7.8 units can be calculated. Serendipitously, this value is closer to the $I^{L(C)}$ value of 7.6 units than to the $I^{L(N)}$ (17.6 units); however, we must keep in mind that the GGA functionals, such as BP86, generally provide an overly covalent electronic structure. For example, a hybrid GGA functional with as much as 40% HF exchange was found to provide the most reasonable electronic structure for aryl-alkyl-thioether in compared with high level *ab initio* wavefunction methods (Rokhsana *et al.*, 2012). A further limitation of the comparison of experimental spectral features and electronic structure calculations for an isolated single TU molecule is the omission of intermolecular interactions (hydrogen bonding, cations) either due to crystal packing or solvation environment.

The MO diagram for $[Ni(TU)_6]^{2+}$ obtained at the BP86/def2-TZVP/PCM(CH_3CN) level for the symmetrized molecule from the crystal structure is presented in Fig. 11(*c*). The S-based free ligand HOMOs (e_g orbitals) are formed from the symmetry adapted linear combinations (SALC) of the six donor lone pairs [Fig. 11(*b*)]. At higher energy, the six C—S π^* orbitals, followed by six C—S σ^* orbitals, can be found. The energy difference between C—S π^* and C—S σ^* decreases from ~2.5 eV in the free ligand to ~0.8 eV when the ligands are coordinated to the Ni^{2+} center. Remarkably, the same reduced energy gap was observed experimentally in the S *K*-XANES spectra when comparing the free and coordinated TU (Figs. 3 and 4).

In $[Ni(TU)_6]^{2+}$, the e_g SALCs combine with the Ni $3d_{z^2}$ and $3d_{x^2-y^2}$ orbitals to form degenerate singly unoccupied molecular orbitals (SUMOs); hence, the triplet $S = 1$ ground state. The next LUMO+3, LUMO+4 and LUMO+5 orbitals show evidence of back-donation into the TU ligand from the occupied Ni orbitals due to their approximately $0.3e^-$ per hole Ni character from AIM analysis. The experimental XANES features corresponding to the back-bonding interactions are expected to show up at the Ni *L*-edges (850–1000 eV). These MOs are followed by a C—S σ^* (LUMO+7) orbital 0.1 eV higher in energy than the highest C—S π^* orbital. Beyond these energies the orbitals mix with diffuse Rydberg orbitals and are not discussed here due to their negligible importance to *M*–*L* covalent bonding.

The MO diagram for the S_4-symmetrized crystal structure of $[Co(TU)_4]^{2+}$ is presented in Fig. 11(*b*). Here, the SALCs of the S lone pairs [HOMOs in Fig. 12(*a*)] donate to the degenerate Co $3d_{xz}$ and $3d_{yz}$ *e*-set of orbitals, whereas the *b*-symmetry HOMO-1 [Fig. 12(*b*)] donates to the Co $3d_{xy}$ orbital, hence,

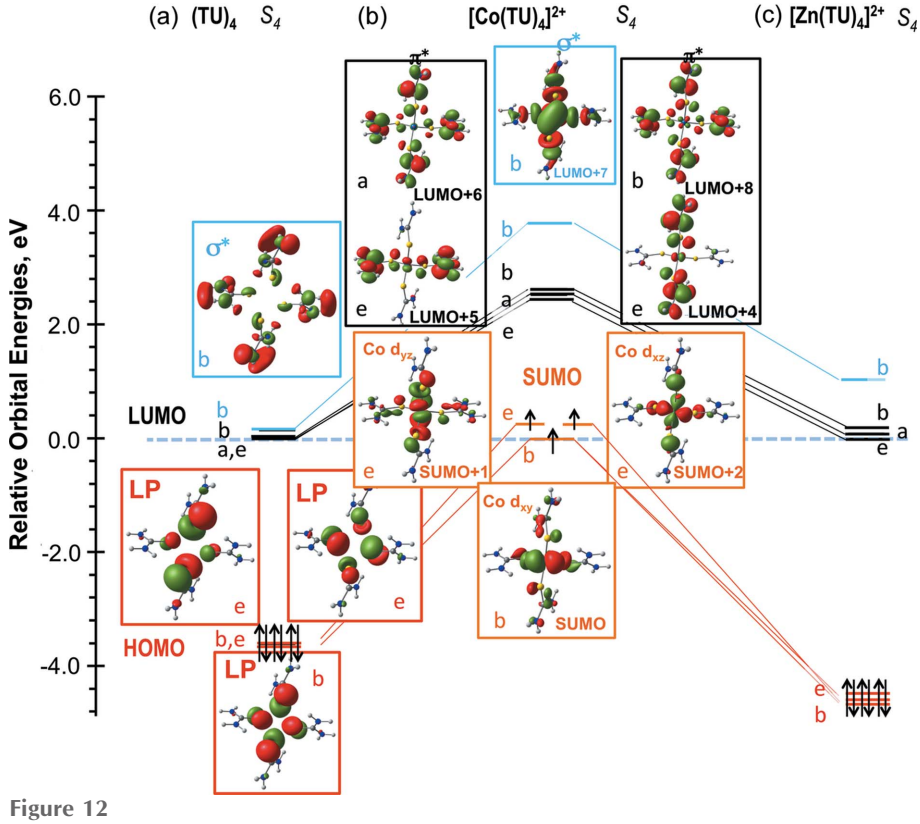

Figure 12
Ground state MO diagram calculated at the BP86/def2-TZVP/PCM(CH_3CN) level for S_4-symmetrized experimental geometries of (*a*) $(TU)_4$, (*b*) $[Co(TU)_4]^{2+}$ and (*c*) $[Zn(TU)_4]^{2+}$.

the quartet S = 3/2 ground state. The SUMOs with e and b symmetries are split by approximately 0.1 eV; however, this is small enough for the ligand field stabilization energy to overcome the energy gain due to exchange stabilization that keeps the electron–electron repulsion minimal by forming three SUMOs. As detected experimentally (Cotton *et al.*, 1964), the S = 1/2 spin ground state was estimated to be 0.74 eV and 0.48 eV higher than the S = 3/2 for the crystal structure and the optimized geometry (see below), respectively. The Co 3*d*-based SUMOs are followed by the C—S π^* orbitals. The LUMO+4 and LUMO+5 orbitals suggest back-donation due to considerable Co content of *ca* 0.3e$^-$ per hole, which can be confirmed from the Co *L*-edge spectra. The energy difference between C—S π^* and C—S σ^* is the same between the Co^{2+} to the Zn^{2+} complexes, which further supports the use of the $[Zn(TU)_4]^{2+}$ spectrum for the most reasonable background correction and rising-edge subtraction of the $[Co(TU)_4]^{2+}$ spectrum as shown in Fig. 10(*b*).

The sulfur atomic contributions to the SUMOs were determined by AIM population analysis (Table 3) using the three representative density functional exchange and correlation functionals. The energy separation of S valence atomic orbitals limits the contribution of the 3*s* to at most a percent. Thus, the total sulfur atomic contribution is the experimentally measurable S 3*p* character from S *K*-XANES. The GGA functional provides the most covalent picture, while the hybrid GGA with approximately 20% HF exchange shows the most ionic bonding. The metaGGA functional follows a mixed trend by being closer to the pure GGA for the Ni^{2+} complex and *vice versa* in the Co^{2+} complex for the hybrid GGA method. The analysis of the S *K*-XANES spectra gave similar pre-edge intensities; however, after renormalization by the number of absorbers (6 *versus* 4) and number of electron holes (2 *versus* 3), the S 3*p* covalency per 3*d* electron-hole of the Ni^{2+} complex is about 9/4 greater than that of the Co^{2+} complex. It is important to highlight that, as found for a more complete series of Ni^{2+} complexes, the spectroscopically sound ground state electronic structure description by DFT-based electronic structure calculations remains challenging.

The AIM-derived S orbital character, average experimental D_0 form Table 2, and equation (1) can be used to calculate the DFT-based transition dipole integral in the complexes (I^C) for $[Ni(TU)_6]^{2+}$ that are 14.9 units, 20.7 units and 16.4 units for BP86, B3LYP and TPSS functionals, respectively. The corresponding I^C values for $[Co(TU)_4]^{2+}$ are 9.56 units, 11.6 units, and 10.5 units, respectively. These transition dipole integrals are all lower than the experimentally derived value from Table 2 [22.2 units or 32.2 units for $I^C(Ni^{2+})$ and 25.1 units or 35.1 units for $I^C Co^{2+}$], which indicate the limitations of DFT to correctly reproduce the experimental *M*–*L* covalency in the ground state of the Ni^{2+} complexes.

Similarly to the free TU ligand where the BP86 calculations may have provided fortuitously correct orbital compositions for the LUMO, the hybrid B3LYP functional here may provide a reasonable Ni—S bond covalency (23% S) that is actually comparable to the experimentally derived S 3*p* character (21%) when using the dipole integral $I^{L(C)}$ for non-conjugated S ligands. This is again a fortuitous agreement, since an extensive computational study for a comprehensive spectroscopic series of [Ni(II)S_4] complexes (Queen *et al.*, 2013) argued that all DFT functionals, including the hybrid B3LYP method, gave too covalent Ni—S bonding. Thus, the experimental S 3*p* character should be less than any of the DFT-based numbers shown in Table 3, which in turn supports the larger value ($I^{L(N)}$) of transition dipole integral for the TU ligand and TU complexes which takes into account the N-based conjugation.

Table 3
Summary of various DFT calculated orbital compositions (percent Ni/Co/S contribution per hole) using the def2-TZVP basis set and PCM(CH_3CN) condensed-phase model from the AIM analyses of the $[Ni(TU)_6]^{2+}$ and $[Co(TU)_4]^{2+}$ complexes.

		Ni†	S	Co‡	S
GGA (BP86)	LUMO+2 (Co $3d_{xy}$)	–	–	66	24
'Rung 2'	LUMO+1 (Ni $3d_{z^2}$ or Co $3d_{yz}$)	60	30	44	18
	LUMO (Ni $3d_{x^2-y^2}$ or Co $3d_{xz}$)	58	34	72	20
	Average for all electron holes	59	32	61	21
	Ratio of Ni/Co S character §	1.52			
metaGGA (TPSS)	LUMO+2 (Co $3d_{xy}$)	–	–	69	22
'Rung 3'	LUMO+1 (Ni $3d_{z^2}$ or Co $3d_{yz}$)	63	26	58	19
	LUMO (Ni $3d_{x^2-y^2}$ or Co $3d_{xz}$)	62	30	57	16
	Average for all electron holes	63	29	61	19
	Ratio of Ni/Co S character §	1.52			
hybrid GGA (B3LYP)	LUMO+2 (Co $3d_{xy}$)	–	–	44	19
'Rung 4'	LUMO+1 (Ni 3d$_z$2 or Co $3d_{yz}$)	66	21	73	16
	LUMO (Ni 3d$_x$2$_{-y}$2 or Co $3d_{xz}$)	66	25	27	18
	Average for all electron holes	66	23	48	18
	Ratio of Ni/Co S character §	1.28			

† Two 3*d* electron holes. ‡ Three 3*d* electron holes. § Experimental ratio from S *K*-XANES (Table 2) is 2.3–2.5.

4. Conclusions

The combined S *K*-edge XANES and DFT study extended a series of previously investigated conjugated N-containing S-donor ligands (Queen *et al.*, 2013) of maleonitrile and dithiocarbamate to TU with a neutral, formally thione S center. The energy position of the S *K*-edge position (E_0) was assigned to that of the free TU ligand at 2474.6 eV (Fig. 3), which was used to establish the free-ligand-based transition dipole integrals ($I^{L(N)}$) of the TU ligand to be 17.6 units. The ligand-based transition dipole integral was used to obtain the experimental composition of the unoccupied frontier molecular orbitals from the normalized pre-edge intensities and edge positions shifts between the free TU ligand ($E_0^{(L)}$) and the $[Ni(TU)_6]^{2+}$ and $[Co(TU)_4]^{2+}$ complexes ($E_0^{(C)}$). S 3*p* covalencies of 0.15e and 0.06e per 3*d* hole were obtained for the Ni—S and Co—S bonds, respectively. In comparison, the Ni^{2+} and Co^{2+}—S(thiolate) bond covalencies were found to be approximately 0.33e and 0.22e per hole in TM tetrathiolate complexes. The lower covalency of the *M*–S(TU) bond relative to the TM–S(thiolate) bonds corresponds to a considerable S → *M* donation and thus the emergence of a partial

thiolate sulfur character for TU upon coordination to a metal center.

As found for a series of $[Ni(II)S_4]^{2-}$ complexes, none of the GGA, hybrid GGA and metaGGA density functionals used in the given study fully reproduced the above TM–S bond covalency. Fortuitously, the BP86 functional gave a good description of the free TU, while the B3LYP functional was in agreement with the S *K*-edge XAS results when the lower value of the dipole integral ($I^{L(C)}$) was used. Despite this coincidental agreement between DFT and XAS results for some, a more general conclusion is that density functionals generally give an overly covalent bonding description for Ni^{2+}—S(ligand) complexes. In turn, this requires the use of the dipole integral developed for the N-conjugated S-ligands to determine the experimental S orbital character of TU and its complexes. In order to further explore the intimate nature of transition dipole integral and the S-ligand composition, we need to evaluate the cause of the excess fluorescence emission intensity in N-containing ligands relative to corresponding non-substituted hydrocarbon-based ligands by resonant inelastic X-ray scattering at the ligand S *K*-edge energy region.

Comparative fits illustrating the model-based fitting uncertainty and a brief vibrational analysis of the free and coordinated TU complexes are shown in the supporting information. Normalized and fitted S *K*-edge XANES spectra, *XYZ* coordinates of optimized molecular structures and formatted checkpoint files can be accessed at ZENODO, https://zenodo.org/record/4770724.

Acknowledgements

The authors acknowledge graduate student stipend support from Pleotint LLC to MSQ. The manuscript was written through contributions of all authors. All authors have given approval to the final version of the manuscript.

Funding information

Research was sponsored by Pleotint LLC, West Olive, Michigan (MSQ). FJ acknowledges the Natural Sciences and Engineering Research Council of Canada (NSERC) (grant No. RGPIN 2016–04546), Canadian Foundation for Innovation (CFI) and the Province of Alberta (Department of Innovation and Science) for their financial support. XAS measurements were carried out at the Stanford Synchrotron Radiation Lightsource (SSRL; proposal No. 3391). Use of the SSRL, SLAC National Accelerator Laboratory, is supported by the US Department of Energy (DOE), Office of Science, Office of Basic Energy Sciences (contract No. DE-AC02-76SF00515). The SSRL Structural Molecular Biology Program is supported by the DOE Office of Biological and Environmental Research, and by the National Institutes of Health (NIH), National Institute of General Medical Sciences (NIGMS) (grant N. P41GM103393). The contents of this publication are solely the responsibility of the authors and do not necessarily represent the official views of NIGMS or NIH.

References

Bader, R. F. W. (1985). *Acc. Chem. Res.* **18**, 9–15.
Bader, R. F. W. (2010). *J. Phys. Chem. A*, **114**, 7431–7444.
Becke, A. D. (1988). *Phys. Rev. A*, **38**, 3098–3100.
Becke, A. D. (1993). *J. Chem. Phys.* **98**, 5648–5652.
Cortesguzman, F. & Bader, R. F. W. (2005). *Coord. Chem. Rev.* **249**, 633–662.
Cossi, M., Barone, V., Cammi, R. & Tomasi, J. (1996). *Chem. Phys. Lett.* **255**, 327–335.
Cotton, F. A., Faut, O. D. & Mague, J. T. (1964). *Inorg. Chem.* **3**, 17–21.
El-Bahy, G. M. S., El-Sayed, B. A. & Shabana, A. A. (2003). *Vib. Spectrosc.* **31**, 101–107.
Feller, D. (1996). *J. Comput. Chem.* **17**, 1571–1586.
Foster, J. P. & Weinhold, F. (1980). *J. Am. Chem. Soc.* **102**, 7211–7218.
Frisch, M. J., Trucks, G. W., Schlegel, H. B., Scuseria, G. E., Robb, M. A., Cheeseman, J. R., Scalmani, G., Barone, V., Mennucci, B., Petersson, G. A., Nakatsuji, H., Caricato, M., Li, X., Hratchian, H. P., Izmaylov, A. F., Bloino, J., Zheng, G., Sonnenberg, J. L., Hada, M., Ehara, M., Toyota, K., Fukuda, R., Hasegawa, J., Ishida, M., Nakajima, T., Honda, Y., Kitao, O., Nakai, H., Vreven, T., Montgomery, J. A. Jr, Peralta, J. E., Ogliaro, F., Bearpark, M., Heyd, J. J., Brothers, E., Kudin, K. N., Staroverov, V. N., Kobayashi, R., Normand, J., Raghavachari, K., Rendell, A., Burant, J. C., Iyengar, S. S., Tomasi, J., Cossi, M., Rega, N., Millam, N. J., Klene, M., Knox, J. E., Cross, J. B., Bakken, V., Adamo, C., Jaramillo, J., Gomperts, R., Stratmann, R. E., Yazyev, O., Austin, A. J., Cammi, R., Pomelli, C., Ochterski, J. W., Martin, R. L., Morokuma, K., Zakrzewski, V. G., Voth, G. A., Salvador, P., Dannenberg, J. J., Dapprich, S., Daniels, A. D., Farkas, Ö., Foresman, J. B., Ortiz, J. V., Cioslowski, J. & Fox, D. J. (2009). *Gaussian 09*. Revision C1. Gaussian Inc., Wallingford, Connecticut, USA.
Fritz, M., Huttner, G. & Zsolnai, L. (1994). *Chem. Ber.* **127**, A4.
Gardenghi, D. J. (2011). *ADRP – Automated Data Reduction Protocol.* Montana State University, Bozeman, MT, USA.
Giles, L. J., Grigoropoulos, A. & Szilagyi, R. K. (2011). *Eur. J. Inorg. Chem.* **2011**, 2677–2690.
Hedman, B., Hodgson, K. O. & Solomon, E. I. (1990). *J. Am. Chem. Soc.* **112**, 1643–1645.
Keith, T. A. (2011). *AIMAll*. TK Gristmill Software, Overland Park, KS, USA. http://aim.tkgristmill.com/.
Kennepohl, P., Wasinger, E. C. & DeBeer George, S. (2009). *J. Synchrotron Rad.* **16**, 484–488.
Kumler, W. D. & Fohlen, G. M. (1942). *J. Am. Chem. Soc.* **64**, 1944–1948.
Kutoglu, A., Scheringer, C., Meyer, H. & Schweig, A. (1982). *Acta Cryst.* B**38**, 2626–2632.
Lee, C. T., Yang, W. T. & Parr, R. G. (1988). *Phys. Rev. B*, **37**, 785–789.
Mennucci, B. & Tomasi, J. (1997). *J. Chem. Phys.* **106**, 5151–5158.
Miertuš, S., Scrocco, E. & Tomasi, J. (1981). *Chem. Phys.* **55**, 117–129.
Neese, F., Hedman, B., Hodgson, K. O. & Solomon, E. I. (1999). *Inorg. Chem.* **38**, 4854–4860.
Pascal, T. A., Wujcik, K. H., Velasco-Velez, J., Wu, C. H., Teran, A. A., Kapilashrami, M., Cabana, J., Guo, J. H., Salmeron, M., Balsara, N. & Prendergast, D. (2014). *J. Phys. Chem. Lett.* **5**, 1547–1551.
Pascual-ahuir, J. L., Silla, E. & Tuñon, I. (1994). *J. Comput. Chem.* **15**, 1127–1138.
Perdew, J. P. (1986). *Phys. Rev. B*, **33**, 8822–8824.
Perdew, J. P., Ruzsinszky, A., Constantin, L. A., Sun, J. W. & Csonka, G. I. (2009). *J. Chem. Theory Comput.* **5**, 902–908.
Queen, M. S., Towey, B. D., Murray, K. A., Veldkamp, B. S., Byker, H. J. & Szilagyi, R. K. (2013). *Coord. Chem. Rev.* **257**, 564–578.
Rokhsana, D., Howells, A. E., Dooley, D. M. & Szilagyi, R. K. (2012). *Inorg. Chem.* **51**, 3513–3524.

Schuchardt, K. L., Didier, B. T., Elsethagen, T., Sun, L. S., Gurumoorthi, V., Chase, J., Li, J. & Windus, T. L. (2007). *J. Chem. Inf. Model.* **47**, 1045–1052.
Seitz, T., Muth, A., Huttner, G., Klein, T., Walter, O., Fritz, M. & Zsolnai, L. (1994). *J. Organomet. Chem.* **469**, 155–162.
Shadle, S. E., Hedman, B., Hodgson, K. O. & Solomon, E. I. (1995). *J. Am. Chem. Soc.* **117**, 2259–2272.
Shadle, S. E., Penner-Hahn, J. E., Schugar, H. J., Hedman, B., Hodgson, K. O. & Solomon, E. I. (1993). *J. Am. Chem. Soc.* **115**, 767–776.
Solomon, E. I., Hedman, B., Hodgson, K. O., Dey, A. & Szilagyi, R. K. (2005). *Coord. Chem. Rev.* **249**, 97–129.
Spofford, W. A. III & Amma, E. L. (1976). *J. Cryst. Mol. Struct.* **6**, 235–258.
Staroverov, V. N., Scuseria, G. E., Tao, J. & Perdew, J. P. (2004). *Phys. Rev. B*, **69**, 075102.
Szilagyi, R. K. (2009). *Encyclopedia of Inorganic Chemistry*, 2nd ed., edited by B. R. King, pp. 1–13. John Wiley.
Szilagyi, R. K., Metz, M. & Solomon, E. I. (2002). *J. Phys. Chem. A*, **106**, 2994–3007.
Tao, J. M., Perdew, J. P., Staroverov, V. N. & Scuseria, G. E. (2003). *Phys. Rev. Lett.* **91**, 146401.
Tomasi, J., Mennucci, B. & Cammi, R. (2005). *Chem. Rev.* **105**, 2999–3094.
Vega, R., López-Castro, A. & Márquez, R. (1978). *Acta Cryst.* B**34**, 2297–2299.
Watson, P. L., Albanese, J. A., Calabrese, J. C., Ovenall, D. W. & Smith, R. G. (1991). *Inorg. Chem.* **30**, 4638–4643.
Weigend, F. & Ahlrichs, R. (2005). *Phys. Chem. Chem. Phys.* **7**, 3297–3305.
Weininger, M. S., O'Connor, J. E. & Amma, E. L. (1969). *Inorg. Chem.* **8**, 424–431.
Wujcik, K. H., Wang, D. R., Pascal, T. A., Prendergast, D. & Balsara, N. P. (2017). *J. Electrochem. Soc.* **164**, A18–A27.
Yamaguchi, A., Penland, R. B., Mizushima, S., Lane, T. J., Curran, C. & Quagliano, J. V. (1958). *J. Am. Chem. Soc.* **80**, 527–529.